

A. ZOUBIR
L. SHAH
K. RICHARDSON
M. RICHARDSON✉

Practical uses of femtosecond laser micro-materials processing

Laser Plasma Laboratory, School of Optics/CREOL, University of Central Florida,
4000 Central Florida Blvd., PO Box 162700, Orlando, FL 32816, USA

Received: 11 December 2002/Accepted: 20 January 2003
Published online: 28 May 2003 • © Springer-Verlag 2003

ABSTRACT We describe several approaches to basic femtosecond machining and materials processing that should lead to practical applications. Included are results on high-throughput deep hole drilling in glasses in ambient air, and precision high-speed micron-scale surface modification of composite materials and chalcogenide glasses. Ablation of soda-lime silicate glass and PbO lead-silicate is studied under three different sets of exposure conditions, for which both the wavelength and pulse duration are varied. Ablation rates are measured below and above the air ionization threshold. The differences observed are explained in terms of self-channeling in the ablated hole. Fabrication of practical devices such as waveguides and gratings is demonstrated in chalcogenide glass.

PACS 79.20.Ds; 61.80.Ba; 81.65.Cf

1 Introduction

Femtosecond laser micromachining has become increasingly important in recent years for many fields, including micro-optics, micro-electronics, micro-biology, and micro-chemistry. Laser ablation, because of its non-contact nature, allows the micromachining and surface patterning of materials with minimal mechanical and thermal deformation. It is now well known that for many of these applications, the femtosecond regime offers advantages over the nanosecond regime. These advantages lie in its ability to deposit energy into a material in a very short time period, before thermal diffusion can occur. As a result, the heat-affected zone, where melting and solidification can occur, is significantly reduced. Smaller feature sizes, greater spatial resolution, and better aspect ratios can hence be achieved.

Another advantage of femtosecond laser micromachining is its versatility in terms of both the materials that can be processed and the type of processing. A variety of materials have been demonstrated to be suitable for femtosecond laser micromachining, such as metals, semiconductors, polymers, oxide ceramics, silica aerogels, optical glasses, and crystals. A variety of processing methods have been used, including the fabrication of photonic crystals [1], waveguides [2], gratings and single mode couplers [3], and the storage of data.

We present the femtosecond laser micromachining of different materials from three perspectives: (i) deep hole penetration in optical glasses and composite materials, (ii) the fabrication of gratings, and (iii) the creation of waveguides in chalcogenide glass As_2S_3 thin films. We characterize the deep hole drilling by measuring the maximum laser penetration depth in a variety of glasses. We investigate the evolution of material expulsion as a function of the hole depth. We characterize waveguides and gratings fabricated by femtosecond laser writing using a standard interferometric microscope.

2 Theoretical background

2.1 Ablation mechanisms

To this date, the mechanisms that govern femtosecond laser ablation are not fully understood. The current understanding is the following [4]: bound and free electrons at the surface layer are excited via multi-photon absorption. Hot electrons are generated, the material becomes ionized and a plasma forms at the surface of the material. The energy is then transferred to the lattice through bond breaking and material expansion.

2.2 Advantages of the femtosecond regime

Because the processes described above are happening on a picosecond time scale, the thermal diffusion into the material is nearly negligible. The thermal relaxation is characterized by the thermal diffusion length D , which is related to the pulse width τ_p by $D = \kappa\tau_p^{1/2}$, where κ is the thermal diffusivity of the material [5]. If D is shorter than the absorption length, the ablation precedes the thermal diffusion, and the material does not have time to melt and resolidify. Better spatial resolution can be achieved.

In addition, in the nanosecond regime, it is generally accepted that ablation begins with the avalanche ionization of surface carriers, which are typically defects or impurities [6]. Due to the non-uniform distribution of surface carriers in dielectrics, experiments have demonstrated that no precisely defined laser-induced damage threshold exists for laser pulses longer than 10 ps. By contrast, ultrashort laser pulses (< 200 fs), with target intensities often in excess of 10^{12} W/cm², are capable of freeing bound electrons via multi-photon ionization (MPI). Thus, experiments have shown that the laser-induced damage threshold of an ultrashort laser

✉ Fax: +1-407/8233-570, E-mail: mrichard@mail.ucf.edu

pulse has a precise value corresponding to the onset of MPI, which is completely determined by the ionization bandgap energy of the target material.

The reasons above make femtosecond micromachining an attractive technique for the fabrication of fine surface structures in transparent materials. In this paper, we demonstrate that femtosecond laser pulses from a regeneratively amplified Ti:Sapphire can be used to drill holes (≥ 1 mm in depth) with high aspect ratios ($\geq 10 : 1$) in transparent materials at atmospheric pressure.

3 Deep hole drilling in silicate glass

3.1 Experiment

We have investigated the laser ablation of two silicate glasses in three different laser ablation scenarios: with a femtosecond laser at 845 nm, with a nanosecond laser at 845 nm, and with a nanosecond laser at 1064 nm. In order to study the influence of the ionization bandgap on laser ablation, we used soda-lime glass (~ 5 eV) and 45 mol % PbO lead-silicate glass (~ 2.5 eV) as ablated materials [7]. Ablation was performed at atmospheric pressure in two regimes, below and above the air ionization threshold intensity, to gauge how air-ionization modifies the hole profile and material removal rate.

The femtosecond laser system was a Kerr-lens mode-locked Ti:Sapphire oscillator regeneratively amplified by a flashlamp pumped Cr:LiSAF amplifier, able to produce 110 fs (FWHM) laser pulses with a Gaussian temporal profile at 845 nm. The second laser was the unseeded Cr:LiSAF regenerative amplifier, which produced long (60 ns) Q-switched pulses, at 845 nm, from which square 10 ns pulses were sliced using an extra-cavity Pockels cell as an electro-optical pulse cutter. The third laser was a flashlamp pumped Q-switched Nd:YAG laser that produced 15 ns (FWHM) Gaussian-shaped laser pulses at 1064 nm. The laser parameters are listed in Table 1.

Each setup was identical, only differing in the laser source: the laser beam was expanded using a 4 : 1 telescope and filtered by an iris. It was then focused to a 100 μm diameter spot onto the target using a fused silica plano-convex lens with a 20 cm focal length. After initial positioning, the focus spot was not moved during the ablation. The holes were drilled parallel to the long axis of thin polished glass plates.

3.2 Results

Optical microscope images of the holes produced by 10^4 laser pulses in soda-lime silicate glass and PbO lead-silicate glass are shown in Figs. 1 and 2.

In Fig. 1, it can be seen that the femtosecond regime produced deeper holes in soda-lime glass than the nanosecond

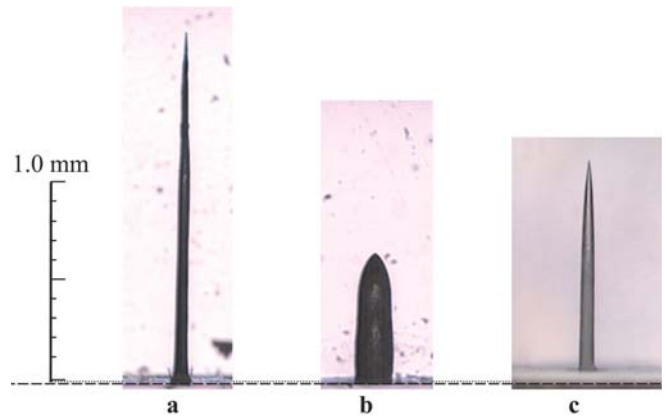


FIGURE 1 Hole profiles in soda-lime glass produced by 10^4 laser pulses: **a** $\lambda = 845$ nm, $t_p = 110$ fs, $E_p = 1.5$ mJ, $I_p = 1.74 \times 10^{14}$ W/cm 2 , $F_p = 19.1$ J/cm 2 ; **b** $\lambda = 845$ nm, $t_p = 10$ ns, $E_p = 4.0$ mJ, $I_p = 5.10 \times 10^9$ W/cm 2 , $F_p = 51.0$ J/cm 2 ; **c** $\lambda = 1064$ nm, $t_p = 15$ ns, $E_p = 2.2$ mJ, $I_p = 1.87 \times 10^9$ W/cm 2 , $F_p = 28.0$ J/cm 2

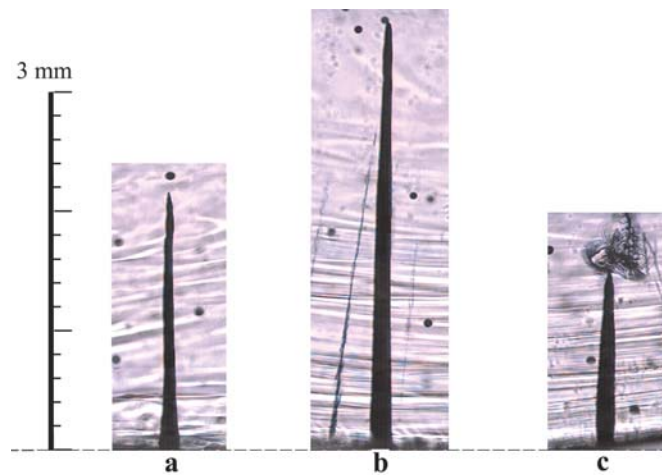


FIGURE 2 Hole profiles in 45 mol % lead silicate glass produced by 10^4 laser pulses: **a** $\lambda = 845$ nm, $t_p = 110$ fs, $E_p = 1.5$ mJ, $I_p = 1.74 \times 10^{14}$ W/cm 2 , $F_p = 19.1$ J/cm 2 ; **b** $\lambda = 845$ nm, $t_p = 10$ ns, $E_p = 4.0$ mJ, $I_p = 5.10 \times 10^9$ W/cm 2 , $F_p = 51.0$ J/cm 2 ; **c** $\lambda = 1064$ nm, $t_p = 15$ ns, $E_p = 2.2$ mJ, $I_p = 1.87 \times 10^9$ W/cm 2 , $F_p = 28.0$ J/cm 2

regime. The differences between the lengths and widths of the holes in Fig. 1b and c illustrate the variation of nanosecond ablation with wavelength: the ionization of surface carriers is highly dependent upon the material ionization bandgap. The avalanche process leading to ablation is initiated by the acceleration of free electrons in the electric field produced by the laser, and is therefore inversely proportional to the laser oscillating frequency. Bass and Barrett demonstrated experimentally that the ablation threshold was larger for nanosecond radiation at 690 nm than at 1.06 μm [8]. Similarly, a lower

Laser	Wavelength λ (nm)	Pulse Duration t_p Pulse Energy E_p	Repetition Rate, R (Hz)	Focal Spot Diameter, D (μm)	Laser Fluence, F_p (J/cm 2)	Focal Intensity, I_p (W/cm 2)
Ti:Saph/Cr:LiSAF	845	110 fs (FWHM) 1.5 mJ	5	100 ($FW1/e^2 M$)	19.1	1.74×10^{14}
Cr:LiSAF	845	10 ns (FWHM) 4.0 mJ	5	100	51.0	5.10×10^9
Nd:YAG	1064	15 ns (FWHM) 2.2 mJ	10	100	28.0	1.87×10^9

TABLE 1 Laser parameters

density and less absorptive electron plasma will be generated by nanosecond pulses at 845 nm than at 1064 nm. Thus, the energy is absorbed over a larger volume and heats a proportionally larger area beyond the vaporization temperature, resulting in a wider, shorter hole.

Figure 2 shows that the overall penetration depth is significantly greater for PbO lead-silicate than for soda-lime silicate glass in the three different ablation scenarios. Due to the presence of high-Z elements in PbO lead-silicate, a higher electron density is obtained beyond the aforementioned wavelength dependence, thus increasing the absorption coefficient in the three cases. It is easier to produce a dense electron plasma and the ablation threshold is therefore lower. In both materials, the femtosecond ablation is more energetically efficient as greater penetration depths are obtained with a smaller energy per pulse. In addition, the dramatic difference between the hole depths and widths in Fig. 1b and c clearly demonstrates the wide variation in nanosecond laser ablation at 845 nm in these glasses. In contrast, Figs. 1a and 2a show that femtosecond laser ablation is much less affected by changes in the target material, because the MPI is significantly less sensitive

to differences in the ionization bandgap than is impurity-seed avalanche ionization.

The same experiment was done in the femtosecond regime with fluences sufficient to ionize the air. The fluence of the laser was increased by reducing the beam spot size from 100 to 75 μm . We compare the femtosecond laser ablation of the two silicate glasses below and above the air ionization threshold in Fig. 3. Below the air ionization threshold, the ablation rate remained constant over the tested range at $\sim 0.2 \mu\text{m}/\text{pulse}$ for both glasses. Above the threshold, the ablation rate rose to $\sim 0.5 \mu\text{m}/\text{pulse}$ and rapidly decreased to $\sim 0.05 \mu\text{m}/\text{pulse}$ (at ~ 1000 shots for soda-lime and ~ 5000 shots for PbO silicate glass). Although the initial and final penetration rates were independent of the target material, the point at which rollover occurred was different for the two glasses studied and indicates that there was a dramatic change in the nature of machining beyond this point [9].

In order to obtain more information about the mechanics of material removal inside the holes, we captured profile images of the laser-produced plasma during laser drilling using a film plate. A small portion of the laser pulse ($\sim 0.1\%$) was converted to $\lambda = 422 \text{ nm}$ using a KD*B frequency doubling crystal, in order to provide a synchronized visible illumination source. The visible light was used to backlight the profile of the hole. The optical probe images, taken during the laser material interaction above ionization threshold, revealed that after a certain depth was achieved, light started to form a thin ($\sim 10 \mu\text{m}$) hot filament confined inside the hole (Fig. 4).

High-intensity ultrashort laser pulses propagating in air have been observed to self-channel into light filaments exceeding the Rayleigh length [10]. It is believed that a similar effect occurs because of evaporated material that remains

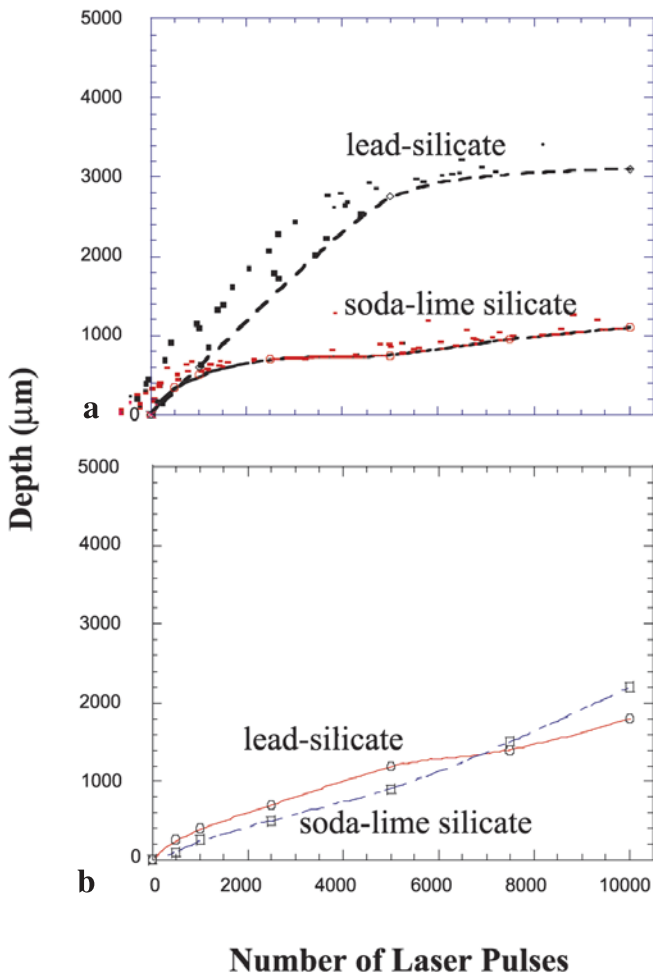


FIGURE 3 Laser penetration depth vs. number of incident laser pulses ($t_p = 110 \text{ fs}$, $\lambda = 845 \text{ nm}$, $E_p = 1.5 \text{ mJ}$) given: **a** $I_p = 3.08 \times 10^{14} \text{ W/cm}^2$, $F_p = 33.9 \text{ J/cm}^2$, and $d = 75 \mu\text{m}$ ($FW1/e^2M$); **b** $I_p = 1.74 \times 10^{14} \text{ W/cm}^2$, $F_p = 19.1 \text{ J/cm}^2$, and $d = 100 \mu\text{m}$ ($FW1/e^2M$)

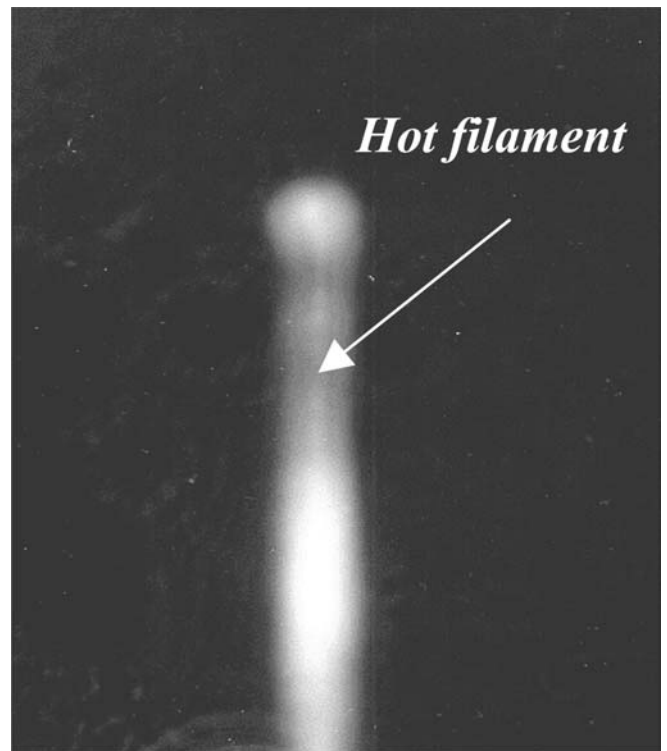


FIGURE 4 Hot filament inside an ablated hole in lead silicate glass



FIGURE 5 Evidence of self-focusing in lead silicate and chalcogenide glass

temporarily confined in the hole, thus increasing the nonlinear index of refraction of the atmosphere. More evidence of this effect is presented in Fig. 5, in which very sharp holes pointing in slightly different directions are shown at the tip of the hole, both in lead silicate glass and As_2S_3 , a chalcogenide glass. These pins could be attributed to ablation due to self-channeled single shots. Note that the individual pins or filaments in the material were uniformly $\sim 100 \mu\text{m}$ long. In addition, it is important to note that the rollover in the ablation rate described above occurred earlier for PbO lead silicate than for soda-lime silicate. We attribute the formation of the hot filament to the presence of high-Z elements (PbO) or particles of highly nonlinear material (As_2S_3) in the hole atmosphere that increase the average nonlinear index of refraction, thus lowering the intensity threshold for self-focusing. This behavior also explains the change in the dynamics of the ablation: the rollover corresponds to the point for which self-focusing occurs, thus decreasing the pointing stability of the ablating beam, as supported by Fig. 5. As a consequence, the ablation rate declines.

4 Hole drilling in composite material

To further illustrate the hole morphology advantages and versatility of femtosecond ablation, ablation was performed on a 3 mm thick graphite fiber composite material. Again ablation was done in both the nanosecond and femtosecond regimes (Fig. 6).

While the nanosecond regime yields dislocations of horizontal and vertical striations indicative of the extent of the heat-affected zone, the femtosecond regime shows a clean, re-

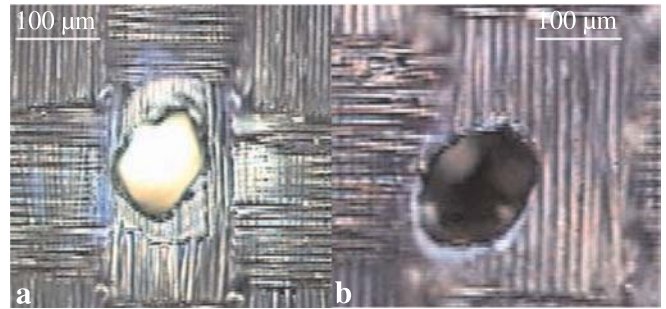


FIGURE 6 $100 \mu\text{m} \times 70 \mu\text{m}$ ablated hole in graphite fiber composite material: **a** 1300 conventional nanosecond laser pulses with $\sim 3.5 \text{ mJ/pulse}$; **b** 100 fs laser pulses with $\sim 1 \text{ mJ/pulse}$

producable hole structure, without evidence of collateral surface damage. The difference in the size of the heat-affected zone is expected to be even greater in laminate materials, in which the heat caused by long pulses can only diffuse in two dimensions versus three in the bulk material.

5 Grating fabrication in As_2S_3 chalcogenide glass thin films

Femtosecond lasers appear to be promising tools for the microstructuring of optical materials. It has been demonstrated that unamplified femtosecond lasers can produce optical breakdown and structural change in bulk transparent materials using tightly focused pulses of just 5 nJ [11].

5.1 Grating fabrication

Using an extended cavity unamplified Kerr-lens modelocked Ti:Sapphire laser, relief and volume gratings with a $20 \mu\text{m}$ period were fabricated on a $1.66 \mu\text{m}$ thick As_2S_3 thin film. The laser emission had a spectral bandwidth of approximately 40 nm (FWHM) centered at 800 nm and a repetition rate of 28 MHz. An interferometric autocorrelation measured a sub-50 fs pulse duration. The system had an average output power of 0.55 W and produced energies up to 20 nJ per pulse. The output of the laser was focused by a $15\times 0.28 \text{ NA}$ reflective objective onto a target attached to a 3D motorized translation system.

The sample was processed in two regimes. Firstly, the intensity was kept below the ablation threshold, generating a volume grating resulting from photoexpansion and an induced index change, as observed through an interferometric

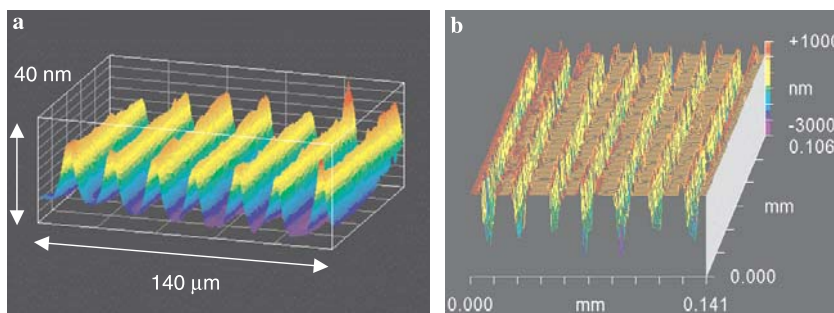


FIGURE 7 Surface profile of **a** the phase and **b** the relief grating on the As_2S_3 film produced with sub-50 fs laser pulses from the extended cavity unamplified Ti:Sapphire oscillator

microscope. In the second regime, intensities above the ablation threshold produced a relief grating with grooves of 0.2 μm depth (Fig. 7).

5.2 Waveguide fabrication

Previous studies have linked bulk glass structural and optical property changes (photosensitivity) through Raman spectroscopy, showing that nonlinear absorption-induced index changes were linked to local bonding changes in As_2S_3 [12]. Following this approach, waveguides over 1 cm in length and $\sim 10 \mu\text{m}$ in diameter were fabricated in As_2S_3 thin films by direct transverse writing using the same unamplified Ti:Sapphire laser (Fig. 8).

Further studies are underway, including the measurement of the refractive index change by the refracted near-field technique. In addition, waveguide Raman spectroscopic measurements in the film will be compared to the previous results in bulk to confirm the molecular bond changes that give rise to the change of the refractive index.

This technique has already established its ability to create complex waveguide structures in optical materials. For instance, directional couplers and 3D-waveguides have been fabricated using a nanojoule laser in borosilicate glass [13] and soda-lime glass. With a reduced complexity of operation and an increased cost-effectiveness, nonlinear material processing with near-IR femtosecond pulses will be of great interest to optical communication systems manufac-



FIGURE 8 Waveguide fabricated with the unamplified Ti:Sapphire laser

turers for the miniaturization and integration of photonic devices.

6 Conclusion

This study has shown the ability of femtosecond material processing to produce very fine surface structures and demonstrated its versatility both in the type of processing and the type of materials that can be processed. Comparison between the femtosecond and nanosecond regimes confirms that finer, more energy-effective and more material-independent structuring can be obtained with femtosecond pulses. The ablation dynamics was described in two types of silicate glasses having different compositions. The differences observed were explained by the self-focusing effect. Examples of device fabrication illustrate the practical use of femtosecond material processing.

REFERENCES

- 1 H.-B. Sun, Y. Xu, S. Juodkazis, K. Sun, M. Watanabe, S. Matsuo, H. Misawa, J. Nishii: *Opt. Lett.* **26**, 325 (2001)
- 2 K. Hirao, K. Miura: *J. Non-Cryst. Solids* **239**, 91 (1998)
- 3 K. Minoshima, A.M. Kowalevich, I. Hartl, E.P. Ippen, J.G. Fujimoto: *Opt. Lett.* **26**, 1516 (2001)
- 4 F. Korte, S. Adams, A. Egbert, C. Fallnich, A. Ostendorf, S. Nolte, M. Will, J.-P. Ruske, B.N. Chichkov, A. Tunnermann: *Opt. Express* **7**, 41 (2000)
- 5 E. Matthias, M. Reichling, J. Siegel, O.W. Kading, S. Petzoldt, H. Skurk, P. Bizenberger, E. Neske: *Appl. Phys. A* **58**, 129 (1994)
- 6 N. Bloembergen: *IEEE J. Quantum Electron.* **QE-10**, 375 (1974)
- 7 Schott Glass Technologies Inc.: *Optical Glass Catalog* (Duryea, PA)
- 8 M. Bass, H.H. Barrett: *Appl. Opt.* **12**, 690 (1973)
- 9 L. Shah: *Femtosecond Laser Micro-Machining of Glasses and Polymers in Air*, Ph.D. Thesis, University of Central Florida (2001)
- 10 A. Braun, G. Korn, X. Liu, D. Du, J. Squier, G. Mourou: *Opt. Lett.* **20**, 73 (1995)
- 11 C.B. Schaffer, A. Brodeur, J.F. Garcia, E. Mazur: *Opt. Lett.* **26**, 93 (2001)
- 12 T. Cardinal, K.A. Richardson, H. Shim, A. Schulte, R. Beatty, K. Le Foulgoc, C. Meneghini, J.F. Viens, A. Villeneuve: *J. Non-Cryst. Solids* **256–257**, 353 (1998)
- 13 A.M. Streltsov, N.F. Borrelli: *Opt. Lett.* **26**, 42 (2001)